DOI: 10.1007/s41230-016-5104-0

Effects of carbon content on high-temperature mechanical and thermal fatigue properties of high-boron austenitic steels

***Xiang Chen [1, 2], Zhi-sheng Wang [1], Yan-xiang Li [1, 2], Hua-wei Zhang [1, 2], and Yuan Liu [1, 2]**

1. School of Materials Science and Engineering, Tsinghua University, Beijing 100084, China

2. Key Laboratory for Advanced Materials Processing Technology, MOE, Beijing 100084, China

Abstract: High-temperature mechanical properties of high-boron austenitic steels (HBASs) were studied at 850 °C using a dynamic thermal-mechanical simulation testing machine. In addition, the thermal fatigue properties of the alloys were investigated using the self-restraint Uddeholm thermal fatigue test, during which the alloy specimens were cycled between room temperature and 800°C. Stereomicroscopy and scanning electron microscopy were used to study the surface cracks and cross-sectional microstructure of the alloy specimens after the thermal fatigue tests. The effects of carbon content on the mechanical properties at room temperature and high-temperature as well as thermal fatigue properties of the HBASs were also studied. The experimental results show that increasing carbon content induces changes in the microstructure and mechanical properties of the HBASs. The boride phase within the HBAS matrix exhibits a round and smooth morphology, and they are distributed in a discrete manner. The hardness of the alloys increases from 239 (0.19wt.% C) to 302 (0.29wt.% C) and 312 HV (0.37wt.% C); the tensile yield strength at 850 °C increases from 165.1 to 190.3 and 197.1 MPa; and the compressive yield strength increases from 166.1 to 167.9 and 184.4 MPa. The results of the thermal fatigue tests (performed for 300 cycles from room temperature to 800 °C) indicate that the degree of thermal fatigue of the HBAS with 0.29wt.% C (rating of 2–3) is superior to those of the alloys with 0.19wt.% (rating of 4–5) and 0.37wt.% (rating of 3–4) carbon. The main cause of this difference is the ready precipitation of $M_{23}(C,B)_6$-type borocarbides in the alloys with high carbon content during thermal fatigue testing. The precipitation and aggregation of borocarbide particles at the grain boundaries result in the deterioration of the thermal fatigue properties of the alloys.

Key words: steel; austenite; boride; high-boron austenitic steel (HBAS); thermal fatigue property

CLC numbers: TG142.25 **Document code:** A **Article ID:** 1672-6421(2016)01-001-08

The temperature of the molding cavities used for molten copper alloys may reach as high as 970 °C during die casting of copper-alloy parts. In addition, the temperature of the mold-cavity surfaces can be as high as 826 °C [1]. Therefore, the service conditions of die-casting molds for copper alloys are far more demanding. Traditionally, hot-work die steels with martensitic matrix, including 3Cr2W8V, H13, THG2000 and QRO90, are commonly used for industrial applications [2-4]. In these steels, strong carbide forming elements as Cr, V, W and Mo are added to form dispersed MC-type precipitates which gives the hot-work die steels excellent strength at elevated temperatures. But owing to the recovery of the tempered martensitic matrix and the coarsening of the alloy carbide precipitates [5-7], the strength of martensitic hot-work die steels will drastically decrease when worked at a high temperature above 650 °C. In order to improve the strength of the steels at temperatures of higher than 650 °C, austenitic hot-work die steels which have no matrix phase transformation are developed [8,9]. However, the austenitic hot-work die steels are still strengthened by MC-type precipitates, and the grains and MC-type precipitates will coarsen at working temperatures [10].

In recent years, high-boron iron-based alloys have attracted much attention as wear-resistant materials [11–18]. Studies have shown that the toughness and strength of the alloy matrix can be increased by replacing eutectic

***Xiang Chen**

Male, born in 1970, Associate Professor. His research and teaching interests are in the areas of cast alloying materials and porous metal materials.

E-mail: xchen@tsinghua.edu.cn

Received: 2015-10-30; Accepted: 2015-12-30

carbides with eutectic borides as the hard, wear-resistant phase to lower the carbon content. The solubility of boron in iron is extremely low (in both austenite and ferrite), while carbon is barely soluble in borides. Moreover, borides have excellent high-temperature tempering stability and do not trend to aggregation [17–20].

Other than the conventional designs of hot-work die steels that strong-carbide-forming elements (such as Mo, V, and W) are added to form dispersed carbides, this new type of high-boron austenitic steels (HBASs) were designed by adding boron to the austenite matrix to form a hard boride phase. The amount of borides in the alloys and the properties of the alloy matrix could be controlled respectively by adjusting the carbon and boron contents in the alloys. Thus, the new materials can be adapted to various working conditions. Research results have shown that at 850 °C, the tensile yield strength and compressive yield strength of HBAS with a carbon content of approximately 0.3 wt.% were 190.3 and 167.9 MPa, respectively [21]. HBASs have great potential for use as low-cost steels for the die-casting of copper alloys. According to the authors' former studies on high-boron iron-based alloys, the carbon content has a great effect on the mechanical properties of high boron-containing alloys [17-19] and the tensile strength and toughness of high-boron iron-based alloys will decrease dramatically when the carbon content exceeds 0.5wt.% [16]. So the influences of carbon content on the properties of the steel are still needed to be clarified. In this paper, the effects of carbon content on the mechanical properties at room temperature and high temperature and thermal fatigue properties of HBASs were investigated.

1 Materials and methods

The charge materials used included electrolytic manganese, ferroboron, ferrosilicon, low-carbon ferrochromium, electrolytic nickel, copper rod, graphite, and pure iron. The steels used for the study were melted in a medium-frequency induction furnace. The melt was superheated to approximately 1,600 °C. After being held at this temperature for 5 min, one third of the melt was cast into a resin bonded sand Y-block with dimensions of 220 mm × 25 mm to get the low-carbon-content HBAS labelled C2. Then graphite particles with the size of about 3 mm were added into the remaining melt in the furnace. The second ingot was poured after melting down and holding at 1,600 °C for 5 min to get the medium-carbon-content HBAS labelled C3. Continuing to add graphite particles into the remaining melt, C4 steel with high carbon content was cast into a Y-block after melting down and holding at 1,600 °C for 5 min.

All the test specimens were cut from the Y-blocks at the same location (75 mm from the bottom) using a wire-cut electrical discharge machine. The heat treatment process of HBASs was relatively simple compared to traditional ones used for the die casting of steels. Diffusion annealing was performed at 930 °C for 3 h for the test specimens, after which six-sided forging at a ratio of 3:1 was performed at 1,150–950 °C. The dimensions of the final forged pieces were 270 mm × 72mm × 22 mm. All the specimens for the microstructural observations and mechanical tests were obtained directly from the forged pieces. The chemical compositions of the test pieces were measured using an optical emission spectrometer (PDA-7000, Shimadzu, Japan), while their boron contents were calculated using inductively coupled plasma-atomic emission spectroscopy (Vista-MPX, Varian, USA). The results are listed in Table 1.

Table 1: Chemical compositions of experimental steels (wt.%)

Steels	C	B	Cr	Mn	Si	Ni	Cu	P	S
C2	0.19	0.54	8.58	6.68	1.17	6.07	0.50	0.012	0.011
C3	0.29	0. 56	8.86	6.71	1.17	6.06	0.49	0.012	0.010
C4	0.37	0.56	8.75	6.59	1.19	6.04	0.49	0.012	0.010

The impact toughness of the specimens at room temperature was measured with an impact tester (ZBC2302-2, SANS, now part of MTS Systems (China) Co., Ltd., China). The ambient temperature during the experiments was 18 °C. Standard Charpy specimens with dimensions of 10 mm × 10 mm × 50 mm and a U-shaped notch with a depth of 2 mm were used. The impact toughness values reported in this paper are averages of three tests. The tensile and compressive properties of the materials at high temperatures were tested using a dynamic thermal-mechanical simulation testing machine (Gleeble 1500D, Dynamic Systems Inc. (DSI), USA). The tensile test specimens were 6 mm in diameter and 120 mm in length, while those for the compressive test were 8 mm in diameter and 12 mm in length. All tests were performed at a loading speed of 0.1 mm·s^{-1} after the specimens were heated for 1 min at 850 °C. All tested results reported in this paper are averages of three tests.

The self-restraint Uddeholm thermal fatigue test was performed for 300 cycles between room temperature and 800 °C. Figure 1 shows the geometry and dimension of the specimen. After the specimens were washed, the surface cracks were checked using a stereomicroscope (SZ61, Olympus, Japan). The specimens subjected to the thermal fatigue experiments were sliced with a precision slicing machine (SYJ-200, MTI Corporation, USA). Next, images of the sections were analyzed to check for microstructural changes induced by the tests. The thermal fatigue properties of the three alloys were analyzed and the extent of their thermal fatigue was determined with respect to the Uddeholm heat-checking standard scales of the Chinese Standard GB/T 15824-2008.

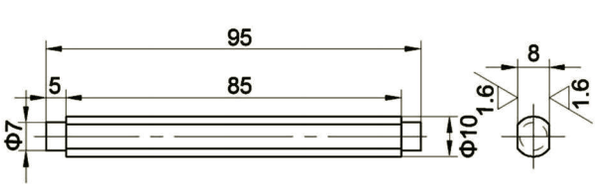

Fig. 1: Geometry and dimension of thermal fatigue specimen (unit: mm)

The HBAS samples were analyzed with a D/max-IIIA X-ray diffraction (XRD) analysis system (Rigaku, Japan) equipped

with a Cu Kα radiation source. The analysis was performed in the 2θ range of 20–80°. The scan rate was 4°·min^{-1} and the step size was 0.02°; the tube voltage was 40 kV and the tube current was 100 mA. The microstructures of the HBAS samples were examined using an optical microscopy (OM) system (NEOPHOT 32, Carl Zeiss Jena GmbH, Germany), a scanning electron microscopy (SEM) system (JSM-6460, JEOL, Japan), and a transmission electron microscopy (TEM) system (JEM-2100, JEOL, Japan). After the specimens had been subjected to coarse grinding and polishing, they were etched in a 3% nital solution. The TEM specimens were sliced into 0.35-mm-thick plates by wire cutting and subsequently ground to a thickness of 50–70 μm with wet 800-grit silicon carbide abrasive paper. The specimens were then punched into foils with a diameter of 3 mm. Finally, these samples were twin-jet electropolished at -15 °C using a standard chromium trioxide-acetic acid solution. The HBAS samples were then analyzed using a nanoprobe for scanning auger electron spectrometry (AES; PHI 700, Physical Electronics Inc. (PHI), USA) equipped with a coaxial electron gun and a cylindrical-mirror electron-energy analyzer. The voltage of the electron gun was 10 kV, the energy resolution was 0.1%, and the incident angle was 30°. The analysis chamber was held at 5.2 × 10^{-7} Pa during the experiments.

2 Results and discussion

3.1 Microstructures and mechanical properties of experimental steels

The as-cast microstructures of HBASs are shown in Fig. 2. The HBASs comprise a dendritic austenite matrix and interdendritic eutectic borides in as-cast condition (Fig. 2a). The morphology of the eutectic borides is in a form of continuous network distribution [Fig. 2(b and c)] and changes to a broken distribution (Fig. 2d) when the carbon content increases to 0.37 wt.%.

The morphology of primary borides are affected by the carbon contents in the HBASs. The carbon element hardly solutes in the borides [12-13], most of the carbon solutes in the austenite which makes the austenite more stable. So with the increasing of carbon content, more chromium and manganese elements dissolved in the austenite matrix would form borides. According to the former studies by the authors [22], with the increase of chromium, the morphology of boride changes from continuous network to less continuous distribution. More isolated borides were observed in the alloy with carbon content of 0.37 wt.%.

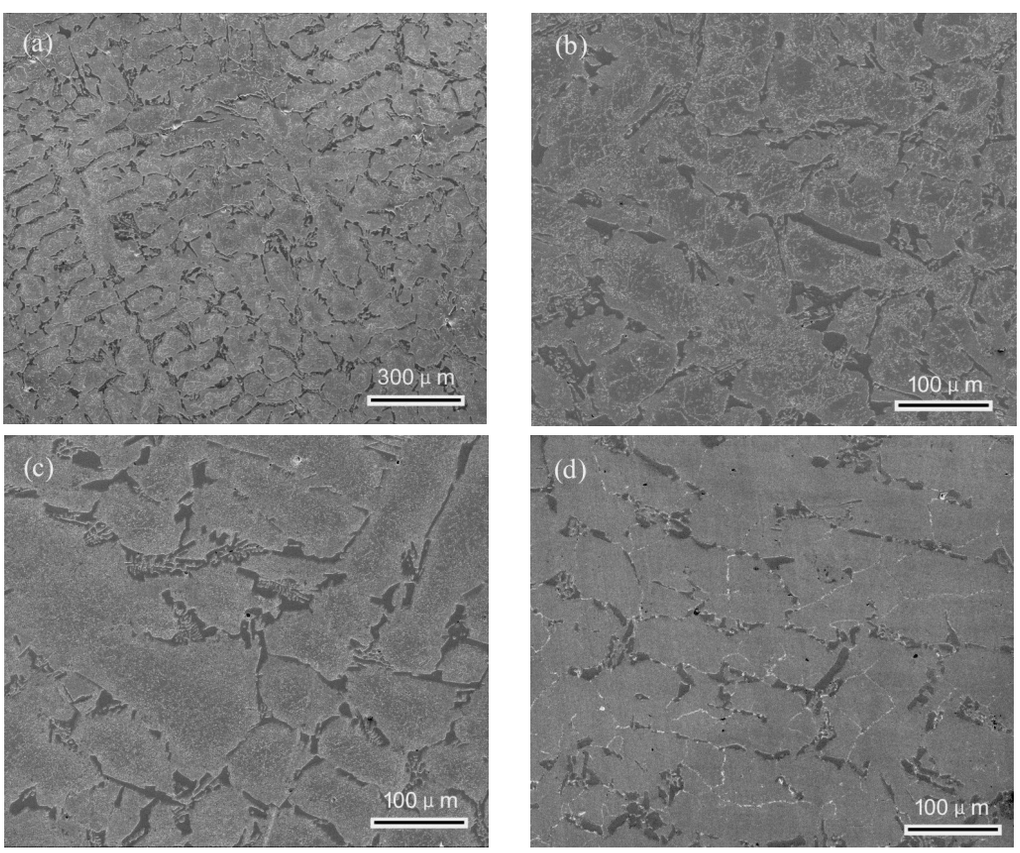

Fig. 2: As-cast micrographs of HBASs: (a) low-magnification image of C2, (b) high-magnification image of C2, (c) high- magnification image of C3, (d) high-magnification image of C4

Figure 3 shows OM images of the experimental HBASs after forging. Pure austenite matrixes were observed in the three alloys. It can also be seen that owing to the high boron content [12, 13, 23–25], a large amount of borides were distributed inside the austenite matrix. No sharp corners were observed in the relatively rounded boride phase [Fig. 3(a, b, c and d)], which was distributed in a discontinuous network with granular discretization. Generally, borides tend to aggregate along

the grain boundaries. The aggregates of borides in the steel specimen C2 [Fig. 3(a and b)] were denser than those in C3 [Fig. 3(c and d)]. OM images of the steel specimen C4 at different magnifications are shown in Fig. 1(e and f). Its boride phase was even smoother than those of C2 and C3 and was scattered uniformly within the matrix in a granular manner. Furthermore, small granular precipitations were scattered in the matrix.

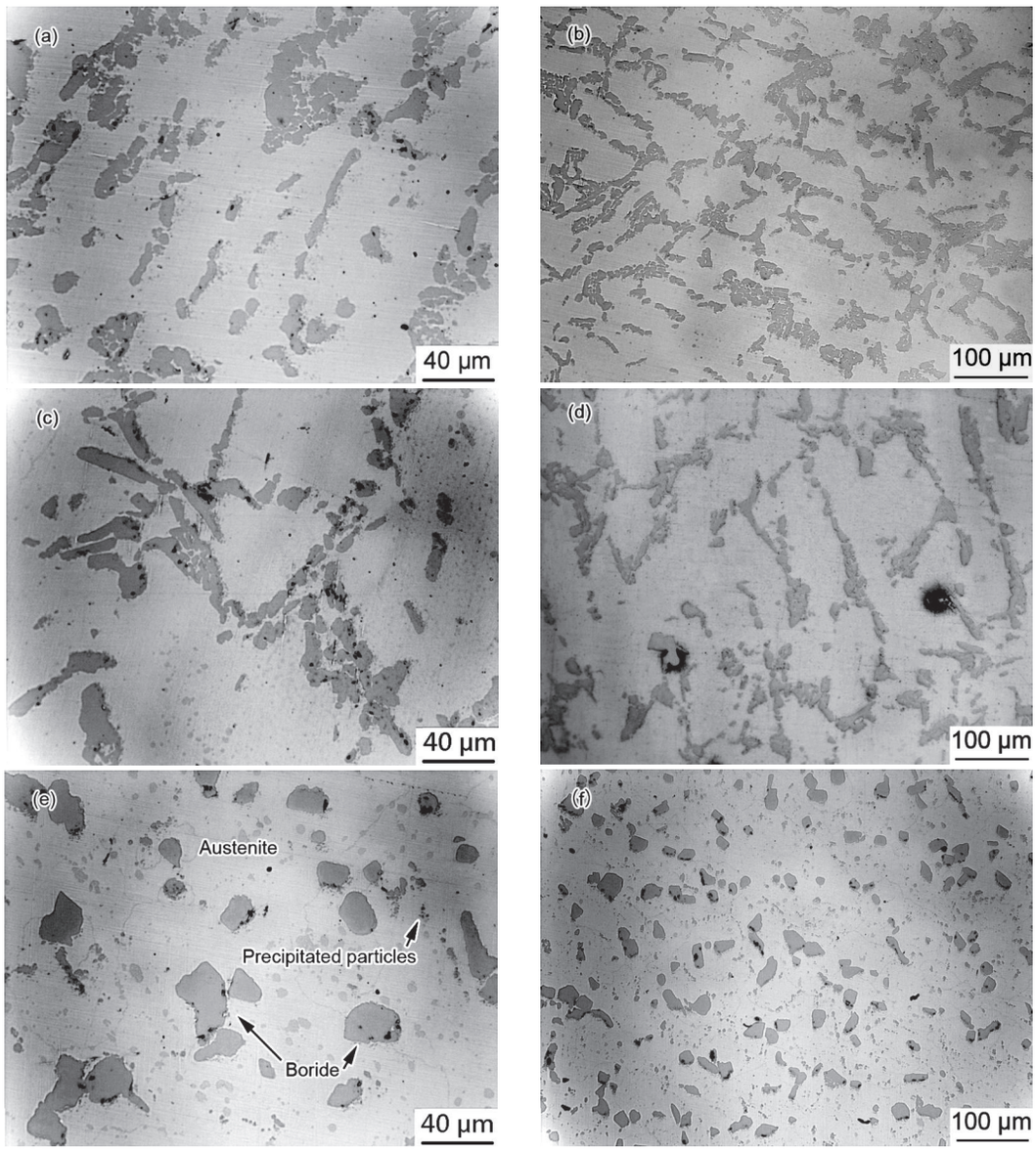

Fig. 3: OM images of HBASs: (a) high-magnification image of C2, (b) low-magnification image of C2, (c) high-magnification image of C3, (d) low-magnification image of C3, (e) high-magnification image of C4 and (f) low-magnification image of C4

Figure 4 shows SEM images of the HBASs after forging. Most of the borides within the matrix of C2 had rounded edges, as can be seen in Figs. 4a and 3a; however, a few of the particles exhibited sharp edges. As mentioned above, borides are usually distributed along the grain boundaries where they tend to aggregate. It can be seen in Figs. 4b and 3c that the edges of the boride particles in C3, which had a carbon content of 0.29wt.%, were more rounded, while a few particles had sharp edges. The borides were distributed along the grain boundaries in a granular and discrete manner and exhibited a lower degree of aggregation than that seen in C2. In contrast, granular precipitations with dimensions of approximately 1 μm were observed within the matrix of C3 (Fig. 4c) and C4 (Fig. 4d).

The XRD spectra of the HBASs, shown in Fig. 5, prove that the matrices of all three alloys consisted of austenite and the major hardening phase was borides. A weak carbide-related peak was observed in the XRD spectrum of C4. This peak was extremely weak in the case of C3. Moreover, such a peak was barely noticeable in the spectrum of C2. When viewed with the previously described microstructural images, the XRD spectra indicate that the small and scattered precipitated particles within the alloy matrix of C3 and C4 belonged to a borocarbide. Ma et al. [24] also found that a high concentration of secondary particles, consisting of a mixture of different borocarbides, precipitated from the dendritic matrix grains.

The results of the AES analysis of C3 are shown in Fig. 6. In Fig. 6a, area 1, located within a boride granule, is the area whose composition was analyzed. It can be seen in Fig. 6b that the main constituent elements of the borides were B, Fe, and Cr; the mole ratios of the elements, as determined by a semiquantitative analysis, were 40.0at% B, 32.5at% Fe, and 24.2at% Cr.

In order to identify the borides and precipitates present in the matrix of C3, TEM analysis was performed. Figure 7 shows the resulting TEM images as well as the selected-area electron diffraction (SAED) pattern and energy-dispersive spectroscopy (EDS) spectra of the borides and precipitates observed with the matrix of C3. The borides were determined to be $Fe_{1.1}Cr_{0.9}B_{0.9}$ (Fig. 7a). Moreover, the borocarbide precipitate particles in the matrix, which can be seen in the bright-field TEM image in Fig. 7b, were confirmed by the SAED pattern to have the crystal structure of $M_{23}C_6$. Thus, it was concluded that the precipitate particles were of a $M_{23}(C,B)_6$-type borocarbide, where M is Fe, Cr, or Mn.

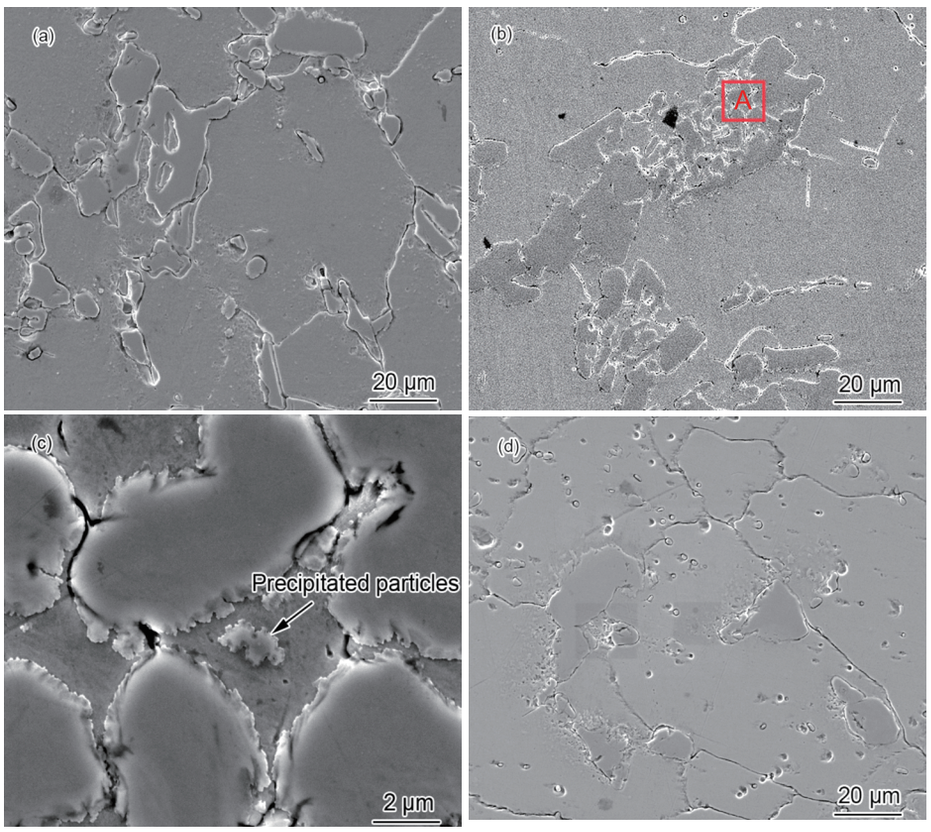

Fig. 4: SEM images of the investigated HBASs: (a) low-magnification image of C2; (b) low-magnification image of C3; (c) enlarged high-magnification image of area A in Fig. 4(b); (d) low-magnification image of C4

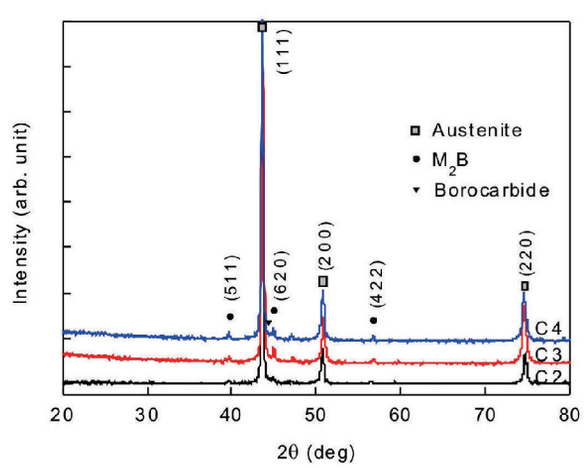

Fig. 5: XRD spectra of investigated HBASs

2.2 Mechanical properties

The mechanical properties of the HBASs at room temperature are shown in Table 2. The hardness of the alloys after forging improved from 239 (C2) to 302 HV (C3) with an increase in the carbon content, while the impact toughness increased from 9.2 to 15.5 J. It can be seen in Figs. 3(e, f, and d) that borides were present within the matrix of C4 and they were more rounded than those present in the matrices of C2 and C3.

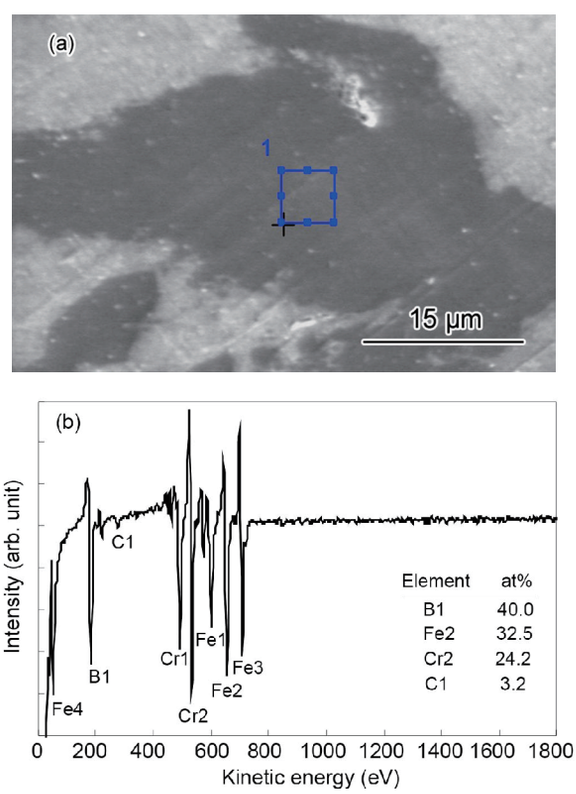

Fig. 6: AES analysis of C3: (a) area tested during composition analysis; (b) constituent elements

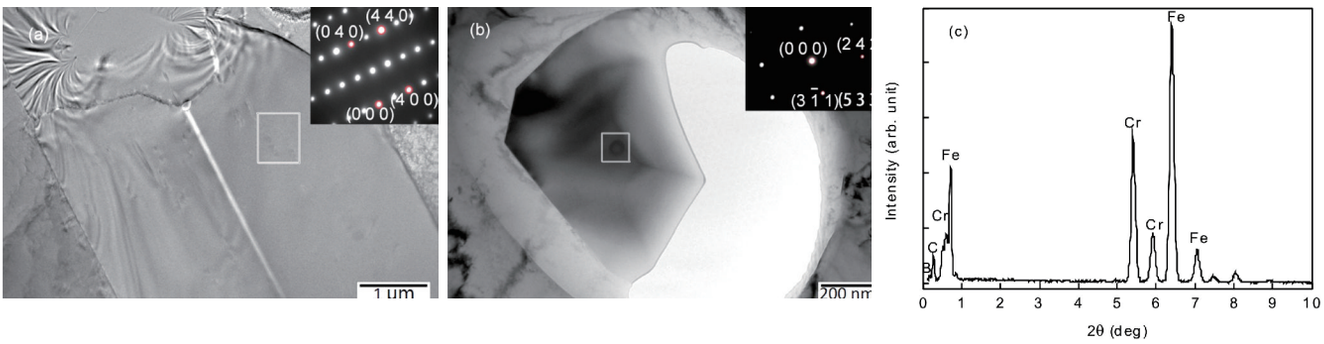

Fig. 7: TEM image, SAED pattern, and ED spectrum for C3: (a) bright-field image and SAED spectrum of boride; (b) bright-field image and SAED pattern of precipitated borocarbide particles; (c) ED spectrum of precipitated borocarbide particles

Table 2: Mechanical properties of investigated HBASs at room temperature

Steel	Hardness (HRC)	Impact toughness (J)
C2	239	9.2
C3	302	15.5
C4	312	16.1

Small precipitated particles and a few peeled-off traces of the precipitated granules were also observed within the matrix. The hardness and impact toughness of C4 were 312 HV and 16.1 J, respectively, which were slightly higher than the values for C3. Thus, the hardness and impact toughness of the HBASs increased significantly with an increase in carbon content from 0.19wt.% to 0.29wt.%. This was because the higher carbon content leads to the higher matrix hardness and rounded borides without sharp corners integrate better with the alloy matrix. Increasing the carbon content from 0.29wt.% to 0.37wt.% also significantly improved the morphology of the borides and their distribution, but it had little effect on the mechanical properties of the alloy, primarily because the borides were already highly rounded and distributed in a discrete manner when the carbon content was 0.29wt.%. Thus, the additional rounding and discretization of the borides did not have a noticeable effect on the impact toughness. As a result, it can also be concluded that the hardness of the investigated HBASs could not be increased significantly without further increasing the amount of borides in the materials.

The high-temperature mechanical properties of the HBASs were tested at 850 °C with a Gleeble 1500D dynamic thermal-mechanical simulation testing machine and the tested results are shown in Table 3. Engineering stress-strain curves for HBASs tested at 850 °C are shown in Fig. 8. It can be concluded from Table 3 and Fig. 8 that, when the carbon content was

Table 3: Mechanical properties of investigated HBASs at 850 °C

Steel	R_m (MPa)	$R_{p0.2}$ (MPa)	A (%)	Z (%)	$R_{p0.2}/R_m$	R_{mc} (MPa)	$R_{pc0.2}$ (MPa)	$R_{pc0.2}/R_{mc}$
C2	183.0	165.1	39.7	48.2	0.90	276.2	166.1	0.60
C3	196.7	190.3	39.2	48.8	0.97	287.4	167.9	0.58
C4	209.6	197.1	36.8	46.9	0.94	290.1	184.4	0.64
H13[21]	130.0	90.4	50.4	77.3	0.69	184.0	116.2	0.63

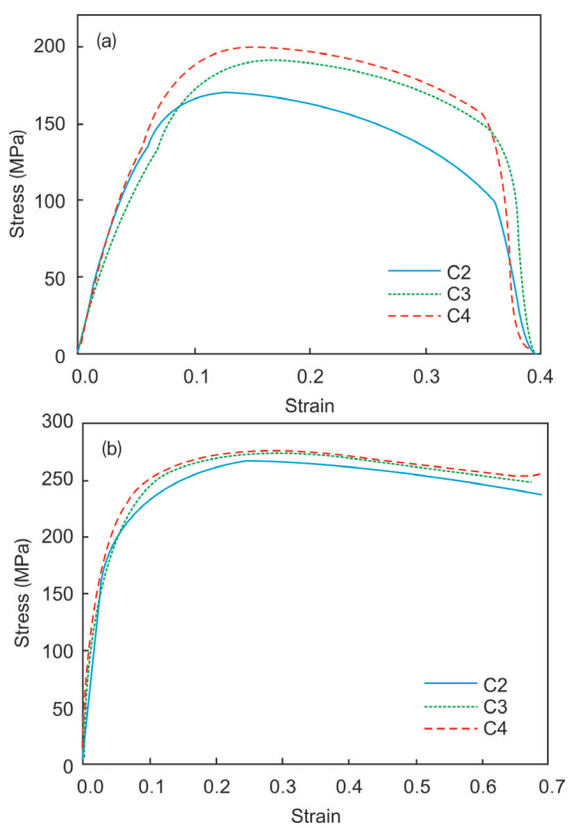

Fig. 8: Engineering stress-strain curves tested at 850 °C in (a) tension and (b) compression

increased, the tensile strength (R_m), tensile yield strength ($R_{p0.2}$), compressive strength (R_{mc}), and compressive yield strength ($R_{pc0.2}$) of the alloys all improved to varying degrees. The yield ratios of C3 and C4 (which had higher carbon content) were slightly higher than that of C2. The percentage elongation (A) and percentage reduction in area (Z) of C4 were both lower than those of C2 and C3. In contrast, the tensile yield strength and compressive yield strength of the commercial steel H13 at 850 °C were 90.4 and 116.2 MPa, respectively. The high-temperature mechanical properties of the HBASs were improved noticeably when the carbon content was increased from 0.19wt.% to 0.29wt.%, while the compressive yield strength were improved when the carbon content was further increased to 0.37wt.%. Thus, a carbon content of approximately 0.3wt.% resulted in the best high-temperature mechanical properties.

2.3 Thermal fatigue properties

The experimental steels were subjected to thermal fatigue testing (Uddeholm method; 300 cycles; temperature varied between room temperature and 800 °C). Stereomicroscopy images of the surface cracks of the test specimens after binarization are shown in Fig. 9. In general, borides are effective in strengthening the austenite matrix because they impede the propagation of thermal fatigue cracks. They also change the direction of crack propagation and prevent the radial extension of thermal cracks [21]. All the steels investigated exhibited good thermal fatigue properties. As shown in Fig. 9a, the cracks on the surface of the C2 specimen after 300 cycles of the test were relatively uniform and penetrated each other, forming a reticular network. The thermal fatigue level of this specimen was determined to correspond to a rating of 4–5 according to Uddeholm heat-checking standard scales of the Chinese Standard GB/T 15824-2008. The cracks on the surface of the C3 specimen were fewer in number and much thinner than those on the surface of the C2 specimen (Fig. 9b). Furthermore, the cracks did not form an interpenetrating reticular network, and the thermal fatigue level of this specimen was determined to correspond to a rating of 2–3. Figure 9c shows that the cracks on the C4 specimen were significantly higher in number than those on the surface of the C3 specimen but slightly lower than those on the surface of the C2 specimen. The primary cracks also interpenetrated each other and formed a reticular network; the thermal fatigue level of this specimen was determined to correspond to a rating of 3–4. And all the HBASs' rating are much better than rating 7–8 of electroslag remelting H13 steel (Fig. 9d) for comparison.

The high-temperature mechanical properties of C4 (carbon content of 0.37wt.%) were slightly better than those of C2 and C3. However, the increasing of the high-temperature mechanical properties was not the case for the improvement of resistance to thermal fatigue of HBASs. C3 (0.29wt.% C) exhibited higher resistance to thermal fatigue than did C4. On one hand, C3 exhibited good high-temperature strength because its borides exhibited a smooth and rounded morphology and were discretely distributed. On the other hand, C4, whose matrix contained 0.37wt.% carbon, was more likely to form $M_{23}(C,B)_6$-type borocarbide precipitates (Fig. 10a). The interface between the borocarbide and the matrix was inferior to that between the boride phase and the matrix, thus negatively affecting the thermal fatigue properties of the alloys. The repeated thermal cycling resulted in the precipitation and aggregation of the boride particles (Fig. 10b), as well as an increase in the volume fraction of the borocarbide phase (Fig. 10c) near the grain boundaries, causing failure of the grain boundaries. Owing to a combination of these two factors, the thermal fatigue properties of C3 were superior to those of C4 (which had a higher carbon content), even though the latter exhibited better high temperature mechanical properties.

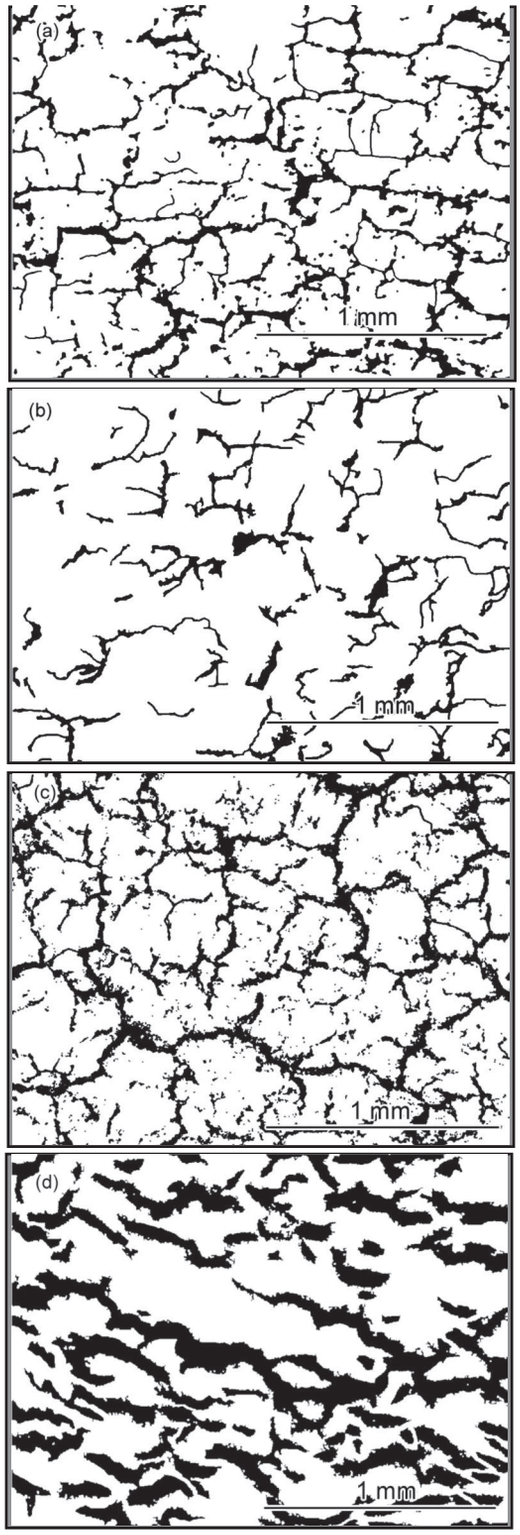

Fig. 9: Cracks on the surfaces of test specimens after 300 cycles of thermal fatigue test from room temperature to 800 °C: (a) C2; (b) C3; (c) C4; (d) H13 [21]

3 Conclusions

(1) The carbon content has a great influence on the morphology of borides in HBASs. When the carbon content in the investigated HBASs was increased from 0.19wt.% to 0.29wt.%, the borides present within the alloy matrix became rounder and were distributed in a discrete manner. Furthermore, when the carbon content was increased from 0.29wt.% to 0.37wt.%, the boride granules became even rounder and their distribution in the matrix became optimized.

(2) Due to the morphology changes of the borides, the increasing of the carbon content improved the

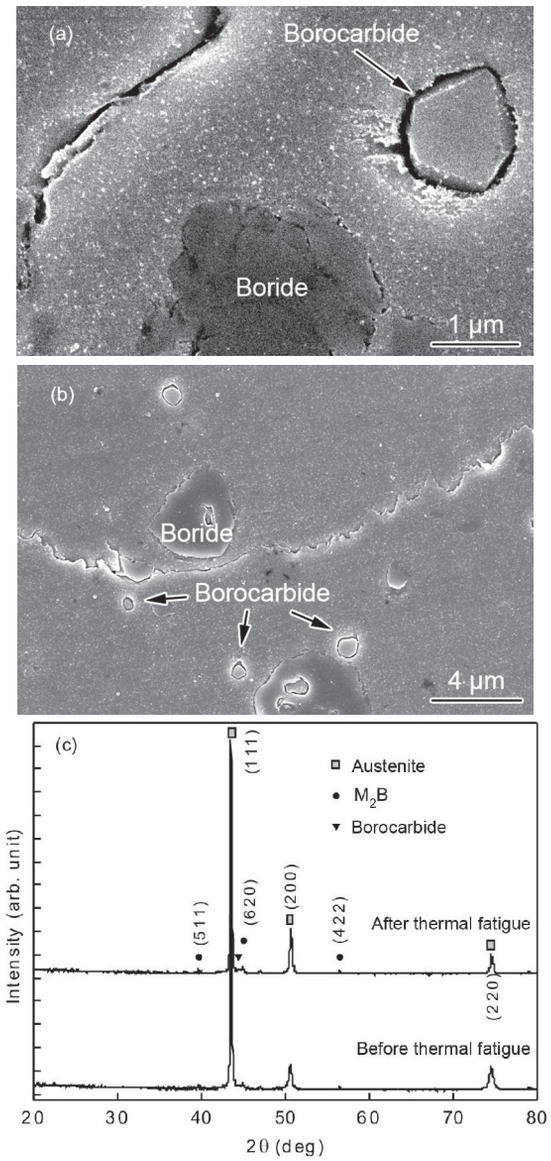

Fig. 10: C4 steel: (a) SEM image before thermal fatigue test; (b) cross-sectional SEM image after 300 cycles of thermal fatigue test from room temperature to 800 °C; (c) XRD spectrum before and after thermal fatigue test

mechanical properties of the alloys both at room temperature and high temperature of 850 °C.

(3) After the thermal fatigue test (300 cycles from room temperature to 800 °C), the thermal fatigue level of the HBAS with 0.29wt.% carbon corresponded to a rating of 2–3, which was higher than that of the alloy with 0.19wt.% carbon (rating of 4–5) and the one with 0.37wt.% carbon (rating of 3–4). Higher carbon content can lead to the precipitation of borocarbide particles, which gradually aggregate near the grain boundaries and cause failure for the repeated thermal cycling, reducing the thermal fatigue resistance. The optimal carbon content for HBASs in the investigated ranges is at about 0.29wt.%.

References

[1] Persson A, Hogmark S, Bergström J. Temperature Profiles and Conditions for Thermal Fatigue Cracking in Brass Die Casting Dies. J. Mater. Process. Technol., 2004, 152: 228–236.
[2] Tsuji N and Abe G. High temperature low cycle fatigue behaviour of a 4.2Cr-2.5Mo-V-Nb hot work tool steel. J. Mater. Sci. Let., 1996, 15: 1251–1254.
[3] Klobčar D, Tušek J and Taljat B. Thermal fatigue of materials for die-casting tooling. Mater. Sci. Eng. A, 2008, 472: 198–207.
[4] Medvedevaa A, Bergströmb J, Gunnarssona S, et al. High-temperature properties and microstructural stability of hot-work tool steels. Mater. Sci. Eng. A, 2009, 523: 39–46.
[5] Norstrom L A, Ohrberg N. Development of hot-work tool steel for high-temperature applications. Met. Technol., 1981, 8: 22–26.
[6] Sjöström J. Chromium martensitic hot-work tool steels — damage, performance and microstructure. Dissertation, Karlstad University Press, Karlstad, 2004.
[7] Michaud P. Tooling Materials and their Applications from Research to Market. In: Proceedings of the 6th International Tooling Conference, Torino, 2006: 733–740.
[8] Jiang H and Wu X C. Research on a new nitrogen-bearing austenitic hot work die steel. Trans. Mater. Heat Treat, 2011, 32: 67–72. (In Chinese)
[9] Hisashi T, Hiroshi H, Yuichi S, et al. Effect of matrix component on the precipitation strengthening of austenitic hot work die steels. J. Iron Steel Inst. Japan, 1981, 67: 1557–1566.
[10] Xie C S, He X S and Cui K. Grain coarsening behaviour towards austenitic hot work tool steels and effect of alloying elements. Acta Metall. Sin., 1986, 22: A461–A469. (In Chinese)
[11] Liu Z L, Li Y X, Chen X, et al. Microstructure and Mechanical Properties of High Boron Iron-based Alloy Solidified in Different Moulds. Acta Metall. Sin., 2007, 43: 477–481. (In Chinese)
[12] Chen X and Li Y X. Effect of Heat Treatment on Microstructure and Mechanical Properties of High Boron White Cast Iron. Mater. Sci. Eng. A, 2010, 528: 770–775.
[13] Chen X, Li Y X and Zhang H M. Microstructure and Mechanical Properties of High Boron White Cast Iron with about 4wt.% Chromium. J. Mater. Sci., 2011, 46: 957–963.
[14] Chen X, Zheng S and Yuan J Y. Microstructures and Mechanical Properties of Austempered Fe-C-Si-B Alloy. Procedia Eng., 2012, 27: 1780–1788.
[15] Liu Z L, Li Y X and Chen X. Effect of Tempering Temperature on Microstructure and Mechanical Properties of High Boron White Cast Iron. China Foundry, 2012, 9: 313–317.
[16] Liu Z L. Research on High Boron White Cast Iron. Dissertation, Tsinghua University, Beijing, 2007. (In Chinese)
[17] Li Y X, Liu Z L and Chen X. Development of boron white cast iron. Inter. J. Cast Metal Res., 2008, 21: 67–70.
[18] Liu Z L, Li Y X and Chen X. Microstructure and Mechanical Properties of High Boron White Cast Iron. Mater. Sci. Eng. A, 2008, 486: 112–116.
[19] Liu Z L, Chen X and Li Y X. High Boron Iron-based Alloy and its Modification. J. Iron Steel Res. Inter., 2009, 16: 37–54.
[20] Chen X and Li Y X. Microstructure and Mechanical Properties of a New Type of Austempered Boron Alloyed High Silicon Cast Steel. China Foundry, 2013, 10: 155–161.
[21] Wang Z S, Chen X, Li Y X, et al. Effects of B on High Temperature Mechanical Properties and Thermal Fatigue Behavior of Copper Die-casting Steel. Acta Metall. Sin., 2015, 51: 519–526. (In Chinese)
[22] Liu Z L, Chen X and Li Y X. Effects of Chromium on Microstructure and Properties of High Boron White Cast Iron. Metall. Mater. Trans., 2008, A39: 636–641.
[23] Guo C Q and Kelly P M. Modeling of Spatial Distribution of the Eutectic M2B Borides in Fe-Cr-B Cast Irons. J. Mater. Sci., 2004, 39: 1109–1111.
[24] Ma S Q, Xing J D, Liu G F, et al. Effect of Chromium Concentration on Microstructure and Properties of Fe-3.5B Alloy. Mater. Sci. Eng. A, 2010, 527: 6800–6808.
[25] Ma S Q, Xing J D, Fu H G, et al. Microstructure and Crystallography of Borides and Secondary Precipitation in 18wt.%Cr-4wt.%Ni-1wt.%Mo-3.5wt.%B-0.27wt.%C Steel. Acta Mater., 2012, 60: 831–843.

The work was financially supported by the National Natural Science Foundation of China (No. 50974080).